Journal of Solid State Chemistry **160,** 450–459 (2001)
doi:10.1006/jssc.2001.9273, available online at http://www.idealibrary.com on IDEAL®

$Nb_{28}Ni_{33.5}Sb_{12.5}$, a New Representative of the *X*-phase

Meitian Wang and Arthur Mar[1]

Department of Chemistry, University of Alberta, Edmonton, Alberta, Canada T6G 2G2

Received February 27, 2001; in revised form May 24, 2001; accepted June 8, 2001

The first ternary compound in the Nb–Ni–Sb system, $Nb_{28}Ni_{33.5}Sb_{12.5}$, has been synthesized and its structure has been determined by single-crystal X-ray diffraction methods. $Nb_{28}Ni_{33.5(2)}Sb_{12.5(2)}$ adopts the *X*-phase structure type (orthorhombic, space group *Pnnm*, $Z = 1$, $a = 13.2334(5)$ Å, $b = 16.5065(7)$ Å, $c = 5.0337(2)$ Å), which belongs to the set of tetrahedrally close-packed (TCP) structures adopted by many intermetallic compounds. Typical of such TCP structures, the atoms reside in sites of high coordination number, with Ni and Sb in CN12 and Nb in CN14, -15, and -16 sites. The relative importance of various metal–metal bonding interactions is discussed on the basis of extended Hückel band structure calculations. $Nb_{28}Ni_{33.5}Sb_{12.5}$ displays metallic behavior with a room-temperature resistivity of 2.3×10^{-4} Ω cm. © 2001 Academic Press

Key Words: **intermetallics; antimonide; crystal structure; band structure.**

INTRODUCTION

Ternary antimonides *RE*–*M*′–Sb containing a rare earth (or Group 3 transition metal) and a late transition metal have attracted attention because of their potential for displaying interesting magnetic properties (1), and more recently, because of their promising thermoelectric properties, especially in $RE Fe_{4-x}Co_xSb_{12}$ (RE = La, Ce; $0 < x < 4$) compounds (2). In contrast, ternary antimonides *M*–*M*′–Sb containing an early (Groups 4–6) and a late transition metal have not been as extensively investigated. In the (Zr, Hf)–(Ni, Pd, Pt)–Sb systems, several compounds have been characterized: *M*NiSb (M = Zr, Hf; Co_2Si-type) (3), MNi_2Sb (M = Zr, Hf; YPt_2In-type) (4), M_5NiSb_3 (M = Zr, Hf; Ti_5Ga_4-type) (5, 6), $Zr_5Ni_{0.5}Sb_{2.5}$ (Mn_5Si_3-type) (7), $Hf_{10}Ni_xSb_{6-x}$ (W_5Si_3-type) (8), $Hf_6Ni_{1-x}Sb_{2+x}$ (Fe_2P-type) (9), $M_3Ni_3Sb_4$ (M = Zr, Hf) (10), and $Zr_3Pt_3Sb_4$ ($Y_3Au_3Sb_4$-type) (10). In the (Nb, Ta)–(Ni, Pd, Pt)–Sb systems, no ternary compounds have been reported thus far, to our knowledge.

[1] To whom correspondence should be addressed. Fax: (780) 492-8231. E-mail: arthur.mar@ualberta.ca.

The divergence in the crystal chemistry of Group 4 *vs* 5 antimonides is also reflected in the binary compounds. For example, the structures of binary Zr *vs* Nb antimonides are quite different. ZrSb occurs as two phases with FeSi- and ZrSb-type structures (11, 12), whereas NbSb crystallizes only in the NiAs-type structure (13). Two orthorhombic phases of $ZrSb_2$ with Co_2Si- and $ZrSb_2$-type structures are known (12, 14), whereas $NbSb_2$ has a monoclinic structure (15, 16). There are no analogues of Zr_2Sb (La_2Sb-type) (11) and Zr_5Sb_3 (Mn_5Si_3- (LT) and Y_5Bi_3-type (HT)) (17) among the Nb antimonides, while Nb_5Sb_4 (Ti_5Te_4-type) (18) finds no counterpart among the Zr antimonides. However, the structure of Zr_3Sb (Ni_3P-type) (19) can be derived from that of Nb_3Sb (Cr_3Si-type) (18, 20), which represents a simple example of a *tetrahedrally close-packed structure* (21–24).

Tetrahedrally close-packed structures (sometimes called topologically close-packed (TCP) or Frank–Kasper structures) are adopted by a large number of intermetallic compounds of the transition metals, and include well-known examples such as the Laves ($MgCu_2$, $MgNi_2$, $MgZn_2$), A15 (Cr_3Si), and σ (FeCr) phases (21–24). Unlike close-packed structures in which atoms of equal size pack to generate small tetrahedral and large octahedral interstices, TCP structures are realized when two or more types of atoms of slightly different size achieve the best filling of space by packing to form only small, slightly irregular tetrahedral interstices. Moreover, the coordination geometries are limited to four types, with CN12, −14, −15, and −16. While size considerations are important, the valence electron concentration (VEC) is another factor that controls the structure. For instance, inclusion of main-group elements, especially Si and Al, stabilizes some phases (NbNiAl and Nb_2Ni_3Si are hexagonal Laves phases whereas $NbNi_2$ itself does not exist) and destabilizes others (addition of Al to the Cr–Co system inhibits σ-phase formation) (23).

The *X*-phase is an interesting case of a TCP structure which, until now, had only a unique representative, a Si-stabilized intermetallic compound $Mn_{45-x}Co_{40+x}Si_{15}$ whose structure was determined in the early 1970s (25, 26). We describe here the preparation, crystal and electronic

0022-4596/01 $35.00

structures, and electrical resistivity of $Nb_{28}Ni_{33.5}Sb_{12.5}$, a new Sb-stabilized intermetallic compound. To our knowledge, it is only the second compound to crystallize in the *X*-phase structure, and is the first ternary compound found in the Nb–Ni–Sb system.

EXPERIMENTAL

Synthesis

Starting materials were powders of the elements Nb (99.8%, Cerac), Ni (99.9%, Cerac), and Sb (99.995%, Aldrich), and of the binary compound $NbSb_2$ (prepared by direct reaction of Nb and Sb in a 1:2 molar ratio in an evacuated fused-silica tube for 3 days at 800°C). Reaction of Nb, Ni, and $NbSb_2$ in a 1:6:2 molar ratio was carried out in a Centorr 5TA tri-arc furnace under argon (gettered by melting a titanium pellet), followed by heating in a fused-silica tube in a two-zone furnace with a temperature gradient of 900/950°C (charge in cool zone) for 3 days in the presence of trace amounts of iodine. Some small needle-shaped crystals were found in the product, which contained (mol%) 35% Nb, 45% Ni, and 19% Sb, as determined from EDX (energy-dispersive X-ray) analyses on a Hitachi S-2700 scanning electron microscope. The reaction is reproducible. One of these crystals was selected for the structure determination.

After a preliminary structure determination (*vide infra*) was made, reactions of varying stoichiometries were attempted to resolve some compositional ambiguities. Mixtures of Nb, Ni, and either $NbSb_2$ or Sb were arc-melted, and the products were characterized by X-ray powder diffraction on an Enraf-Nonius FR552 Guinier camera (Table 1). Although there is evidence for some degree of nonstoichiometry, which is common for many intermetallic compounds, Table 1 shows that there is consistently a slight excess of Ni over Nb. In conjunction with the single-crystal structure determination, these results suggest that the average composition is close to $Nb_{28}Ni_{32}Sb_{14}$.

TABLE 1
Reactions in the Nb–Ni–Sb System

Reaction	Nb:Ni:Sb molar ratio	Identified crystalline phases[a]
1	36:28:10	Nb_3Sb (*M*) + other binaries (*m*)
2	32:32:10	Nb_3Sb (*M*) + other binaries (*m*)
3	28:36:10	*X*-phase (*M*) + other binaries (*t*)
4	28:32:14	*X*-phase (*M*) + Nb_3Sb (*t*) + other binaries (*t*)
5	28:28:18	Nb_3Sb (*M*) + *X*-phase (*m*) + other binaries (*t*)

[a] Designations: *M*, major phase (70–90%); *m*, minor phase (10–30%); *t*, trace (<10%).

TABLE 2
Crystallographic Data for $Nb_{28}Ni_{33.5}Sb_{12.5}$

Formula	$Nb_{28}Ni_{33.5(2)}Sb_{12.5(2)}$
Formula mass (amu)	6090.14
Space group	*Pnnm* (No. 58)
a (Å)[a]	13.2334(5)
b (Å)[a]	16.5065(7)
c (Å)[a]	5.0337(2)
V (Å^3)	1099.5(1)
Z	1
ρ_{calc} (g cm^{-3})	9.197
Crystal dimensions (mm)	$0.24 \times 0.04 \times 0.02$
Radiation	Graphite-monochromated Mo$K\alpha$, $\lambda = 0.71073$ Å
μ(Mo$K\alpha$) (cm^{-1})	284.01
Transmission factors	0.241–0.558
2θ limits	$4° \le 2\theta(\text{Mo}K\alpha) \le 65°$
Data collected	$-18 \le h \le 19$, $-24 \le k \le 24$, $-7 \le l \le 7$
No. of data collected	10,904
No. of unique data, including $F_o^2 < 0$	2171
No. of unique data, with $F_o^2 > 2\sigma(F_o^2)$	1670
No. of variables[b]	109
$R(F)$ for $F_o^2 > 2\sigma(F_o^2)$[c]	0.033
$R_w(F_o^2)$[d]	0.083
Goodness of fit	1.039
$(\Delta\rho)_{max}$, $(\Delta\rho)_{min}$ (e Å^{-3})	3.08, −3.40

[a] Obtained from a refinement constrained so that $\alpha = \beta = \gamma = 90°$.
[b] Including an extinction coefficient.
[c] $R(F) = \sum||F_o| - |F_c||/\sum|F_o|$.
[d] $R_w(F_o^2) = [\sum[w(F_o^2 - F_c^2)^2]/\sum wF_o^4]^{1/2}$; $w^{-1} = [\sigma^2(F_o^2) + (0.0399p)^2 + 0.0000p]$, where $p = [\max(F_o^2, 0) + 2F_c^2]/3$.

Structure Determination

The singularity of a selected needle-shaped crystal, its Laue symmetry *mmm*, and preliminary cell parameters were revealed by Weissenberg photography. X-ray diffraction data were collected on a Bruker P4/RA/SMART CCD diffractometer at room temperature with a combination of ϕ rotations (0.3°) and ω scans (0.3°) in the range $4° \le 2\theta(\text{Mo}K\alpha) \le 65°$. Final cell parameters were refined from least-squares analysis of 5952 reflections. Crystal data and further details of the data collection are given in Table 2. All calculations were carried out using the SHELXTL (Version 5.1) package (27). Conventional atomic scattering factors and anomalous dispersion corrections were used (28). Intensity data were processed, and face-indexed absorption corrections were applied in XPREP.

Among the possible space groups (*Pnn*2, *Pnnm*) consistent with the orthorhombic symmetry and systematic absences observed, the centrosymmetric space group *Pnnm* was chosen which led to successful structure solution and refinement. An initial model (model A, "$Nb_{36}Ni_{28}Sb_{10}$") was proposed for the assignment of the 16 independent sites (Table 3), the positions of all of which were readily located

TABLE 3
Models in Refinement of *X*-Phase Structure

	Model A	Model B	Model C	Model D
CN12				
Site 1 (8*h*)	Ni	Ni	Ni	Ni(1)
Site 2 (8*h*)	Ni	Ni	Ni	Ni(2)
Site 3 (4*g*)	Ni	Ni	Ni	Ni(3)
Site 4 (4*g*)	Ni	Ni	Ni	Ni(4)
Site 5 (4*g*)	Ni	Ni	Ni	Ni(5)
Site 6 (4*g*)	Sb	Sb	Sb	Sb(1)
Site 7 (2*a*)	Sb	Sb	Sb	Sb(2)
Site 8 (8*h*)	Nb	Ni	50% Ni, 50% Sb	$X(1) = 59\%$ Ni, 41% Sb
Site 9 (4*g*)	Sb	Sb	Sb	$X(2) = 21\%$ Ni, 79% Sb
CN14				
Site 10 (4*g*)	Nb	Nb	Nb	Nb(1)
CN15				
Site 11 (4*g*)	Nb	Nb	Nb	Nb(7)
CN16				
Site 12 (4*g*)	Nb	Nb	Nb	Nb(2)
Site 13 (4*g*)	Nb	Nb	Nb	Nb(3)
Site 14 (4*g*)	Nb	Nb	Nb	Nb(4)
Site 15 (4*g*)	Nb	Nb	Nb	Nb(5)
Site 16 (4*g*)	Nb	Nb	Nb	Nb(6)
Formula	$Nb_{36}Ni_{28}Sb_{10}$	$Nb_{28}Ni_{36}Sb_{10}$	$Nb_{28}Ni_{32}Sb_{14}$	$Nb_{28}Ni_{33.5(2)}Sb_{12.5(2)}$
R_1/wR_2	0.037/0.103	0.063/0.236	0.038/0.104	0.033/0.083

by direct methods. At this stage, we noted its isotypy to the *X*-phase ($Mn_{45-x}Co_{40+x}Si_{15}$) (25, 26), in which all four kinds of coordination polyhedra (CN12 (icosahedron), CN14, CN15, CN16) possible in a TCP structure are found. Since main-group atoms normally occupy the CN12 sites in TCP structures, the assignment of Sb at these locations is reasonable. A broad principle governing the formation of TCP structures is that transition metals to the right of Group 7 prefer the CN12 sites, those to the left of Group 7 prefer the sites of higher CN, and those in Group 7 (Mn, Tc, Re) have no clear preference (29). Model A conforms well to this principle, except that a CN12 site (site 8) is occupied by Nb and the resulting Nb–Ni distances are generally somewhat shorter than expected. Although refinement on model A proceeded satisfactorily, resulting in reasonable displacement parameters for all atoms including Nb in site 8, attempts at synthesis at the composition "$Nb_{36}Ni_{28}Sb_{10}$" failed, giving only binary products (Table 1). In model B, site 8 is instead occupied by Ni, in compliance with the CN12 site preference for later transition metals, giving the formula "$Nb_{28}Ni_{36}Sb_{10}$." Although a synthesis based on this composition afforded the ternary Nb–Ni–Sb compound in large amounts, refinement of this model was unsatisfactory, yielding unusually small displacement parameters for site 8. Despite their different sizes, there is precedence for disorder of Ni and Sb, as occurs in the crystal structure of Hf_6NiSb_2, for instance (9). In model C, such a disorder was now allowed and occupancies of 50% Ni and 50% Sb were arbitrarily assigned in site 8. The refinement proceeded well and, more convincingly, a synthesis based on the composition "$Nb_{28}Ni_{32}Sb_{14}$" gave the best yield of the ternary phase thus far.

Possible further disorder was next probed in all remaining sites. Prior to this stage (model C), the CN12 (icosahedral) sites are occupied by Ni atoms (sites 1–5), Sb atoms (sites 6, 7, 9), or a mixture of both (site 8), while the CN14, CN15, and CN16 sites (sites 10–16) are occupied by Nb atoms. Since sites 1–5 (Ni) make contacts of $\sim$2.5 Å with sites 6, 7, or 9 (Sb), which are too short for Nb–Sb or Sb–Sb bonds, the possibility of disorder in sites 1–5 could be ruled out. For sites 6, 7, or 9, we considered models involving either Ni/Sb or Nb/Sb disorder; all refinements resulted in essentially 100% Sb occupancy in sites 6 and 7 but in a 21% Ni, 79% Sb occupancy ratio in site 9. The disorder of Ni and Sb in site 8 has already been discussed above. Finally, refinements allowing disorder of Nb with either Sb or Ni in sites 10–16 resulted in 100% occupancy by Nb. Other refinements did not support models allowing Nb or Sb deficiencies or Nb/Ni disorder. We accept as our final model one in which only sites 8 and 9 feature disorder of Ni and Sb atoms, giving the formula $Nb_{28}Ni_{33.5}Sb_{12.5}$ (model D), which is very close to "$Nb_{28}Ni_{32}Sb_{14}$" (model C). The final difference electron density map is featureless ($\Delta\rho_{max} = 3.08$; $\Delta\rho_{min} = -3.40$ e Å^{-3}). The atomic positions were

TABLE 4
Positional and Equivalent Isotropic Displacement Parameters for $Nb_{28}Ni_{33.5(2)}Sb_{12.5(2)}$

Atom	Wyckoff position	x	y	z	U_{eq} (Å^2)[a]
Nb(1)	4*g*	0.02254(6)	0.57316(4)	0	0.01147(16)
Nb(2)	4*g*	0.08693(6)	0.73064(4)	0	0.00749(15)
Nb(3)	4*g*	0.09989(5)	0.16209(4)	0	0.00659(15)
Nb(4)	4*g*	0.21753(6)	0.44618(4)	0	0.00753(15)
Nb(5)	4*g*	0.27940(5)	0.26523(4)	0	0.00664(15)
Nb(6)	4*g*	0.40087(5)	0.55016(4)	0	0.00597(15)
Nb(7)	4*g*	0.59926(6)	0.02495(4)	0	0.00940(16)
Ni(1)	8*h*	0.09926(6)	0.32456(5)	0.23441(15)	0.00839(16)
Ni(2)	8*h*	0.40816(6)	0.39308(4)	0.23934(15)	0.00885(17)
Ni(3)	4*g*	0.19180(9)	0.00229(6)	0	0.0104(2)
Ni(4)	4*g*	0.44436(8)	0.13723(6)	0	0.0084(2)
Ni(5)	4*g*	0.69464(8)	0.29083(6)	0	0.0096(2)
Sb(1)	4*g*	0.50370(4)	0.28599(3)	0	0.00653(12)
Sb(2)	2*a*	0	0	0	0.00720(16)
X(1)[b]	8*h*	0.28595(4)	0.10484(3)	0.24949(11)	0.00796(19)
X(2)[c]	4*g*	0.75676(5)	0.14668(3)	0	0.00591(19)

[a] U_{eq} is defined as one-third of the trace of the orthogonalized U_{ij} tensor.
[b] 59(2)% Ni, 41% Sb.
[c] 21(2)% Ni, 79% Sb.

standardized with the use of the program STRUCTURE TIDY (30). Final values of the positional and equivalent isotropic displacement parameters are given in Table 4. Further data, in the form of a CIF, have been sent to Fachinformationszentrum Karlsruhe, Abt. PROKA, 76344 Eggenstein-Leopoldshafen, Germany, as supplementary material No. CSD-411929 and can be obtained by contacting FIZ (quoting the article details and the corresponding CSD numbers).

Electrical Resistivity

An ingot of dimensions $1.25 \times 0.25 \times 0.09$ mm, taken from the product of reaction 3 (Table 1), was mounted in a four-probe configuration for an ac resistivity measurement between 5 and 300 K on a Quantum Design PPMS system equipped with an AC-transport controller (Model 7100). A current of 0.01 mA and a frequency of 16 Hz were used.

Band Structure

A tight-binding band structure calculation in the extended Hückel approximation was performed on the idealized structure "$Nb_{28}Ni_{32}Sb_{14}$" (model C) with use of the EHMACC suite of programs (31, 32). The atomic parameters used (3, 33) are listed in Table 5. Properties were extracted from the band structure using 45 *k*-points in the irreducible portion of the Brillouin zone.

TABLE 5
Extended Hückel Parameters

Atom	Orbital	H_{ii} (eV)	ζ_{i1}	c_1	ζ_{i2}	c_2
Nb	5*s*	− 8.62	1.890			
	5*p*	− 4.79	1.850			
	4*d*	− 9.28	5.750	0.6401	1.640	0.5516
Ni	4*s*	− 8.62	1.930			
	4*p*	− 4.28	1.930			
	3*d*	− 11.06	5.750	0.5862	2.200	0.5845
Sb	5*s*	− 18.79	2.323			
	5*p*	− 11.70	1.999			

RESULTS AND DISCUSSION

Composition

Although the nominal composition "$Nb_{28}Ni_{33.5}Sb_{12.5}$" found from the structure determination is consistent with the EDX analyses and is close to the starting composition of the synthesis, there is evidence for a narrow range of homogeneity. The variability in composition originates from disorder of Ni and Sb in only two sites in the crystal structure. On the basis of synthetic experiments (Table 1), the composition of this ternary phase is estimated to be $Nb_{28}Ni_{34\pm2}Sb_{12\pm2}$. Lattice constants range from $a = 13.210(8)$ Å, $b = 16.469(9)$ Å, $c = 5.013(3)$ Å, $V = 1090.5(8)$ Å^3 for the ternary phase synthesized in reaction 3 (loading composition $Nb_{28}Ni_{36}Sb_{10}$) to $a = 13.256(6)$ Å, $b = 16.537(7)$ Å, $c = 5.040(2)$ Å, $V = 1104.9(6)$ Å^3 for that synthesized in reaction 4 (loading composition $Nb_{28}Ni_{32}Sb_{14}$). The lattice constants for the single crystal of $Nb_{28}Ni_{33.5}Sb_{12.5}$ analyzed (Table 2) are intermediate between these values. The variation in cell volume in $Nb_{28}Ni_{34\pm2}Sb_{12\pm2}$ is ~1.3%, comparable to the ~1.5% variation in $Hf_6Ni_{1-x}Sb_{2+x}$ ($0 < x < 0.24$) (9). In contrast to the isotypic $Mn_{45-x}Co_{40+x}Si_{15}$, where two or all three components were proposed to be disordered over 9 of the 16 sites, the greater differentiation in atomic sizes in $Nb_{28}Ni_{34\pm2}Sb_{12\pm2}$ may account for the reduction in disorder.

Crystal Structure

Although a large number of alloys and intermetallic compounds crystallize in TCP structures, which include the ubiquitous Laves phases, to date only about 20 TCP structure *types* are known (34), despite the prediction of the existence of many more (21, 22). $Nb_{28}Ni_{33.5}Sb_{12.5}$ is only the second representative of the *X*-phase, which is the structure type adopted by $Mn_{45}Co_{40}Si_{15}$ discovered in 1962 (35) and characterized independently by two groups in 1970 and 1972 (25, 26).

Like most TCP structures, the structure of $Nb_{28}Ni_{33.5}Sb_{12.5}$ can be described in terms of the stacking of

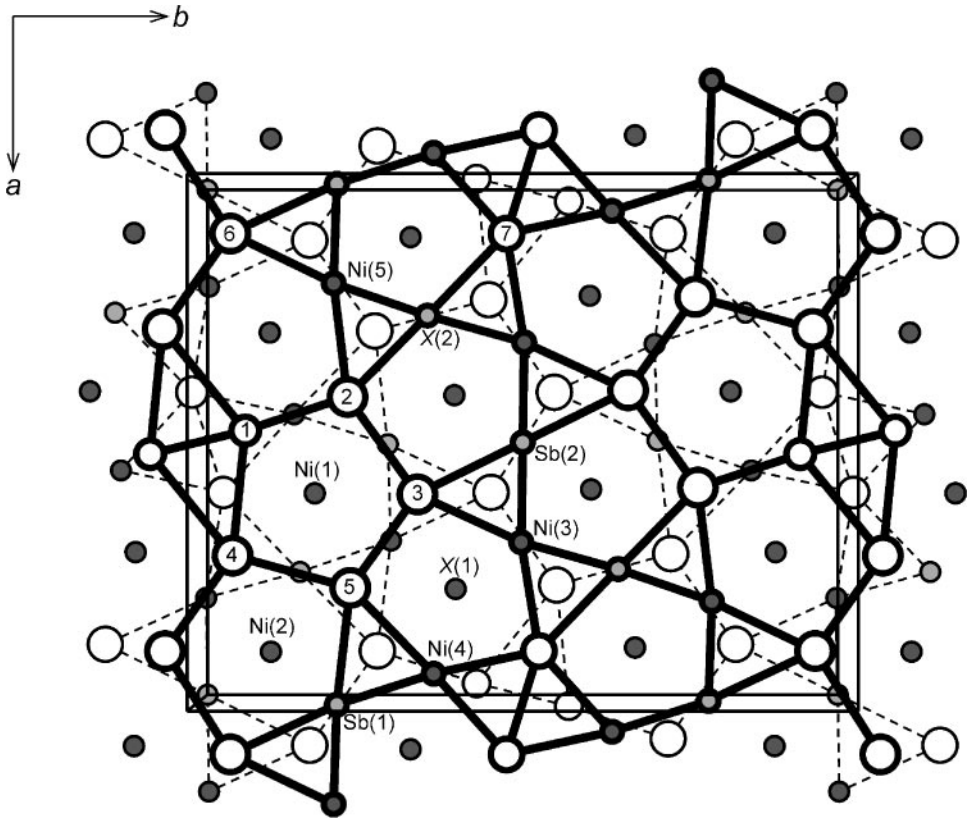

FIG. 1. View down the c axis of the structure of $Nb_{28}Ni_{33.5}Sb_{12.5}$ showing the unit cell outline and the labeling scheme. The open circles are Nb atoms, the solid circles are Ni atoms, and the lightly shaded circles are Sb atoms. For the disordered sites, the more Ni-rich site $X(1)$ is portrayed like a Ni atom and the more Sb-rich site $X(2)$ like an Sb atom. The size of the circles is proportional to the CN of the site. The main layers **A** lie at $z = 0$ (dashed lines) and $z = \frac{1}{2}$ (thick lines), while the secondary layers **B** lie at $z = \sim\frac{1}{4}$ and $\sim\frac{3}{4}$ (unconnected Ni(1), Ni(2), and $X(1)$ sites).

two-dimensional nets. Figure 1 shows the stacking of these layers projected along the short c axis. (For simplicity, the more Ni-rich disordered site $X(1)$ is portrayed like a Ni atom (small solid circles), and the more Sb-rich disordered site $X(2)$ like an Sb atom (small lightly shaded circles).) The primary or main layers **A** (or **A**′), which lie on the $z = 0$ or $z = \frac{1}{2}$ planes, alternate with the secondary layers **B**, which lie on the $z = \sim\frac{1}{4}$ or $z = \sim\frac{3}{4}$ planes, as shown in Fig. 2a. Layers **A** and **A**′ are related by a two-fold screw axis along c. (The standardization of atomic coordinates in the crystal structure of $Nb_{28}Ni_{33.5}Sb_{12.5}$ shifts the origin of the unit cell by $\frac{1}{2}\vec{c}$ relative to that of $Mn_{45}Co_{40}Si_{15}$ so that the layers **A** and **A**′ are interchanged.) Each main layer **A** is constructed from a tessellation of pentagons and triangles whose vertices are Nb, Ni, and Sb atoms and described by the Schäfli symbols $5^3.3 + 5^2.3^2 + 5.3.5.3^2 + 5.3.5.3$, as shown in Fig. 2b. Each secondary layer **B** is constructed from a tessellation of squares and triangles whose vertices are Ni atoms only and described by the Schäfli symbols $4.3^5 + 4.3^4 + 3^6$, as shown in Fig. 2c. It should be understood that the stacking of layers is merely a way of describing and classifying structures, and is not meant to make implications about bonding. While the lines shown in the main layer **A** range from 2.5 to 3.3 Å and do imply bonding contacts, those in the secondary layer **B** are all greater than 4.2 Å and therefore cannot represent bonds; on the other hand, there do exist strong bonding interactions between atoms in the **A** and **B** layers even though they are not drawn.

The coordination polyhedra found in $Nb_{28}Ni_{33.5}Sb_{12.5}$ are shown in Fig. 3, and correspond to the four possible Frank–Kasper polyhedra of CN12, -14, -15, and -16 (29). All CN12 sites, approximately icosahedral (I_h), are occupied by the Ni and Sb atoms. Three of these, Ni(1), Ni(2), and the Ni-rich disordered site $X(1)$, have two opposing vertices that are symmetry equivalents of the central atom. These are also the three sites that make up the secondary **B** layer. If these opposing vertices are considered to be capping atoms of a pentagonal antiprism, then the structure of $Nb_{28}Ni_{33.5}Sb_{12.5}$ can also be regarded as consisting of infinite columns, aligned along the c axis, of pentagonal antiprisms centred by these atoms, as can be seen by inspection of Fig. 1. The CN14 site, occupied by Nb(1), centers a bicapped hexagonal antiprism (approximately D_{6d}) with the six-fold improper rotation axis oriented vertically, and the CN15 site,

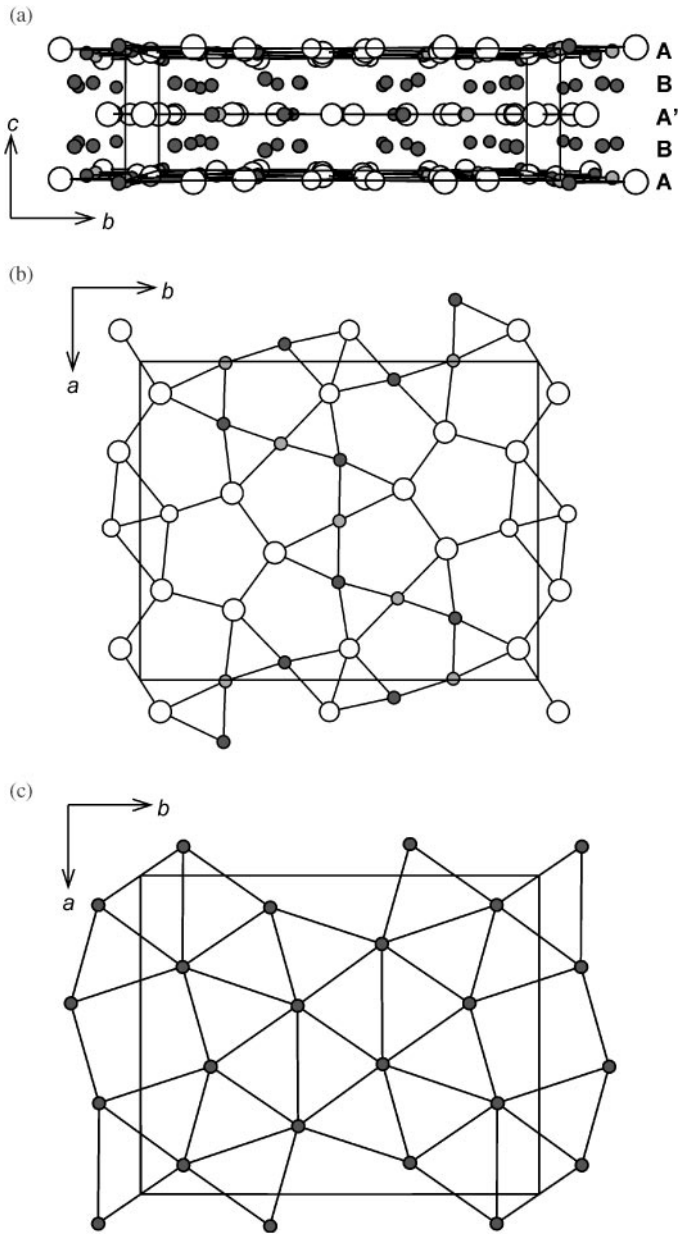

FIG. 2. (a) View down the *a* axis of $Nb_{28}Ni_{33.5}Sb_{12.5}$ showing the stacking of main (**A** and **A**′) and secondary (**B**) layers. (b) Tessellation of pentagons and triangles in main layer **A**. (c) Tessellation of squares and triangles in secondary layer **B**.

occupied by Nb(7), centers a so-called "μ-phase polyhedron" (approximately D_{3h}) with the three-fold rotation axis oriented horizontally in Fig. 3. All CN16 sites, occupied by the remaining Nb atoms, center Friauf polyhedra (approximately T_d).

Interatomic distances found in $Nb_{28}Ni_{33.5}Sb_{12.5}$ are listed in Table 6, to be read downward so that the number of distances corresponds to the CN in the header row. These distances are generally about $\sim$0.2 Å greater than those in $Mn_{45}Co_{40}Si_{15}$, reflecting the larger atomic sizes of the components in $Nb_{28}Ni_{33.5}Sb_{12.5}$. Most Ni–Ni distances lie in the range of 2.449(1)–2.674(2) Å, consistent with that found in elemental Ni (2.49 Å) (36) or NiSb (2.56 Å) (37). The two somewhat shorter distances of 2.360(2) (Ni(1)–Ni(1)) and 2.410(2) Å (Ni(2)–Ni(2)), close to the sum (2.31 Å) of the Pauling single bond radii (38) and corresponding to the repeat of pentagonal antiprisms in the columns along the *c* axis described earlier, may be a result of matrix effects arising from satisfying the packing requirements of atoms in the other coordination polyhedra. Most Nb–Nb distances lie in the range of 2.736(1)–3.324(1) Å, similar to that found in elemental Nb (2.86 Å) (36) or Nb_3Sb (2.63–3.22 Å) (18). There is an unusually short distance of 2.488(2) Å (Nb(1)–Nb(1)) which corresponds to the length of the shared edge of two triangles in the main layer **A** (Fig. 1 or Fig. 2b). A Nb–Nb distance of 2.58 Å is found in Nb_3Ge (39), while (multiply-bonding) distances as short as 2.20 Å are seen in organometallic complexes such as $Nb_2(hpp)_4$ (40). The corresponding Mn–Mn distance in $Mn_{45}Co_{40}Si_{15}$ is also much shorter than the other ones and may be more a result of geometrical constraints imposed by the rest of the structure. There are no Sb–Sb contacts present; the short *X*(1)–*X*(1) distances of 2.512(1)–2.522(1) Å can be interpreted as Ni–Sb contacts given that the *X*(1) site consists of a nearly equal mixture of Ni and Sb. The other Ni–Sb distances of 2.449(1)–2.5915(8) Å are similar to that found in NiSb (2.60 Å) (37). The Nb–Sb distances of 2.8786(9)–2.9922(5) Å are similar to those in $NbSb_2$ (2.84–2.97 Å) and the Nb–Ni distances of 2.616(1)–3.038(1) Å are somewhat longer than those in $NbNi_3$ ($TiAl_3$-type) (2.56–2.59 Å) (41).

Although complex, the *X*-phase structure has been related through a "fourling" operation of units of the simpler $MnZn_2$-type structure, one of the three Laves phases (20, 42). Both consist of main layers tessellated by pentagons and triangles, but whereas the secondary layer in the *X*-phase structure is tessellated by squares and triangles, it is only tessellated by triangles in the $MnZn_2$-type structure. Distortion of the squares in the secondary net of the *X*-phase structure (Fig. 2c) would be necessary to transform it to the 3^6 net found in the $MnZn_2$-type structure.

Electronic Structure

$Nb_{28}Ni_{33.5}Sb_{12.5}$ displays metallic behavior with a small resistivity ratio ($\rho_{300} = 2.3 \times 10^{-4}$ Ω cm, $\rho_5 = 1.6 \times 10^{-4}$ Ω cm, $\rho_{300}/\rho_5 = 1.4$) typical of disordered alloy structures (Fig. 4). This observation is consistent with the band structure calculation (based on an idealized "$Nb_{28}Ni_{32}Sb_{14}$" model), which reveals a moderate density of states (DOS) at the Fermi level ($\varepsilon_f = -9.38$ eV), as shown in Fig. 5. The DOS curve can be decomposed into a rather broad Nb *d*-block, extending from -6 to -12 eV (Fig. 5a), in which only half of these states are occupied, and a narrow block

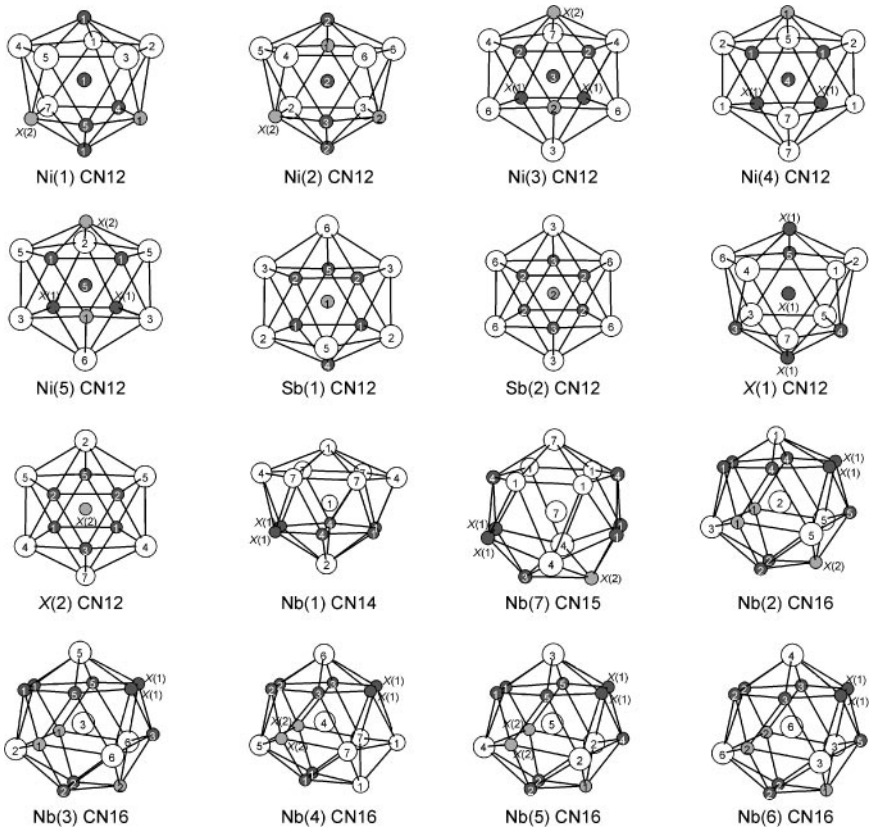

FIG. 3. Coordination polyhedra in $Nb_{28}Ni_{33.5}Sb_{12.5}$.

located just below the Fermi level extending from -10 to -12 eV (Fig. 5b), which represents filled states composed almost entirely of Ni 3*d* character. The substantial mixing of Nb and Ni character from -12 eV up to the Fermi level implies a significant degree of Nb–Ni bonding. Lower down in energy (-12.5 to -14 eV) is a region composed largely of Sb 5*p* character (Fig. 5c) corresponding to Nb–Sb and Ni–Sb bonding levels.

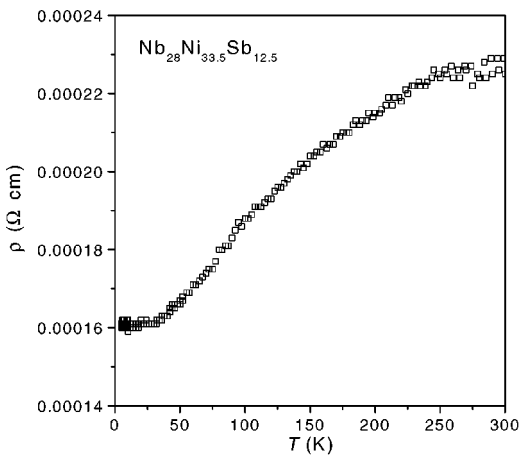

FIG. 4. Temperature dependence of the resistivity of $Nb_{28}Ni_{33.5}Sb_{12.5}$.

The strength of the bonding interactions can be quantified by inspection of their crystal orbital overlap population (COOP) curves (43) (Fig. 6) and their Mulliken overlap populations (MOP) (Table 7). (Note that it is valid to compare overlaps only between identical types of contacts.) The regions centered around the two maxima around -7.5 and -9.5 eV in the Nb *d*-block in the DOS curve (Fig. 5a) correspond to Nb–Nb bonding and antibonding levels, respectively, as verified by inspection of the COOP curve (Fig. 6a). With most of the Nb–Nb bonding levels occupied, all Nb–Nb contacts less than 3.4 Å represent fairly strong interactions, as evidenced by a MOP of 0.267. Although most of the Nb–Nb contacts range from 2.9 to 3.4 Å, with a cumulative MOP of 0.245, there are three that are significantly shorter with substantially larger MOP values: 0.550 for the 2.488(2) Å (Nb(1)–Nb(1)) contact, and 0.417 for the 2.736(1) (Nb(1)–Nb(2)) and 2.753(2) Å (Nb(7)–Nb(7)) contacts. The Nb–Ni (Fig. 6b) and Nb–Sb interactions (Fig. 6c) are optimized in the structure, with all bonding levels just filled up to the Fermi level, and MOP values of 0.097 and 0.271, respectively. Consistent with the preference for the icosahedral sites to be occupied by atoms

TABLE 6
Interatomic Distances (Å) in $Nb_{28}Ni_{33.5(2)}Sb_{12.5(2)}$[a]

	Ni(1) CN12	Ni(2) CN12	Ni(3) CN12	Ni(4) CN12	Ni(5) CN12	Sb(1) CN12	Sb(2) CN12	*X*(1) CN12	*X*(2) CN12	Nb(1) CN14	Nb(7) CN15	Nb(2) CN16	Nb(3) CN16	Nb(4) CN16	Nb(5) CN16	Nb(6) CN16
Ni(1) CN12	2.360			2.527^2	2.647^2	2.592^2			2.521^2	2.616^2	2.821^2	2.880^2	2.930^2	2.806^2	2.834^2	
	2.674															
Ni(2) CN12		2.410	2.593^2			2.485^2	2.513^4		2.483^2			2.986^2	2.998^2	2.930^2	2.968^2	2.861^2
		2.624														2.952^2
Ni(3) CN12		2.593					2.538^2	2.449	2.551		2.801		2.905	2.938^2		2.909^2
Ni(4) CN12	2.527					2.578		2.501		2.765^2	2.739	2.980^2			3.038	
											2.764					
Ni(5) CN12	2.647					2.528		2.453	2.517			2.912	2.917^2		2.907^2	2.913
Sb(1) CN12	2.592	2.485		2.578	2.528							2.934^2	2.948^2		2.988	2.985
Sb(2) CN12		2.513	2.538										2.984			2.957^2
X(1) CN12			2.449^2	2.501^2	2.453^2			2.512		2.879^2	2.911^2	2.955^2	2.921^2	2.907^2	2.932^2	2.918^2
								2.522								
X(2) CN12	2.521	2.483	2.551		2.517						2.895	2.895		2.992^2	2.922^2	
Nb(1) CN14	2.616			2.765^2				2.879		2.488	3.093^2	2.736		3.193		
											3.160^2			3.324		
Nb(7) CN15	2.821		2.801	2.739				2.911	2.895	3.093^2	2.753			3.002^2		
				2.764						3.160^2						
Nb(2) CN16	2.880	2.986		2.980^2	2.912	2.934^2		2.955	2.895	2.736			3.041		3.129^2	
Nb(3) CN16	2.930	2.998	2.905		2.917^2	2.948^2	2.984^2	2.921				3.041			2.923	3.122^2
Nb(4) CN16	2.806	2.930	2.938^2					2.907	2.922^2	3.193	3.002^2				3.097	2.972
										3.324						
Nb(5) CN16	2.834	2.968		3.038	2.907^2	2.988		2.932	2.922^2			3.129^2	2.923	3.097		
Nb(6) CN16		2.861	2.909^2		2.913	2.985	2.956^4	2.918					3.122^2	2.972		3.103
		2.952														

[a] ESDs range from 0.0005 to 0.0015 Å. When read down, the number of distances listed (superscripts indicate number of times a distance occurs) corresponds to the CN in the header row.

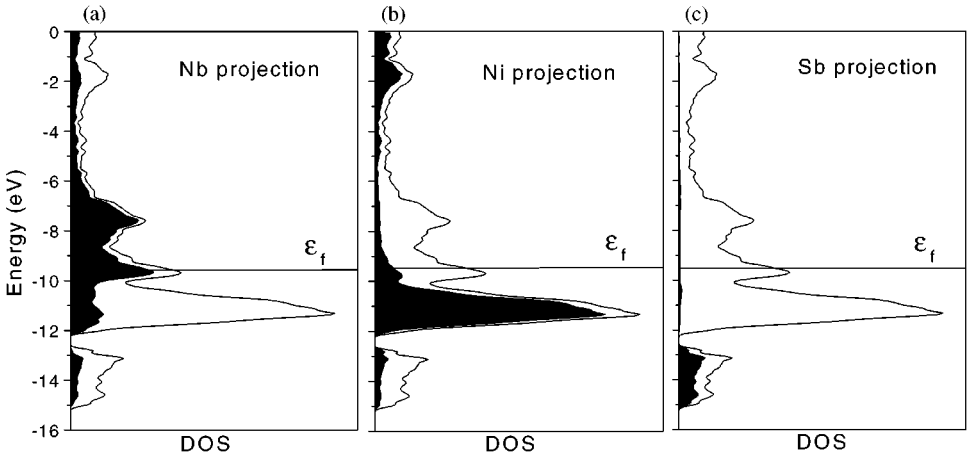

FIG. 5. Contributions of (a) Nb, (b) Ni, and (c) Sb (shaded regions) to the total density of states (DOS) (line) for $Nb_{28}Ni_{33.5}Sb_{12.5}$ (idealized as "$Nb_{28}Ni_{32}Sb_{14}$"). The Fermi level (ε_f) is at -9.38 eV.

with complete *d* subshells, the Ni *d*-block is nearly filled (Fig. 5b); although filling of Ni–Ni bonding levels is nearly canceled by the filling of Ni–Ni antibonding levels (Fig. 6d), these apparently d^{10}–d^{10} interactions (44) also include sufficient mixing of Ni 4*s* and 4*p* states as well as Sb states to stabilize Ni–Ni bonding levels by a small amount so that there is net bonding, as indicated by the small but positive MOP of 0.050. Finally, there are strong Ni–Sb bonds (MOP 0.222) notwithstanding the occupation of some Ni–Sb antibonding levels (Fig. 6e).

Although atomic sizes and packing considerations govern the crystal structure adopted by an intermetallic compound, these are not the only factors. The relative atomic sizes in $Nb_{28}Ni_{33.5}Sb_{12.5}$ and $Mn_{45}Co_{40}Si_{15}$ are quite different, and yet they adopt the same structure. The similarity in valence electron concentrations of $Nb_{28}Ni_{33.5}Sb_{12.5}$ (7.26 e^-) and $Mn_{45}Co_{40}Si_{15}$ (7.35 e^-) is quite striking, and suggests that electronic factors are important. A second-moment scaling treatment of the band structure may prove illuminating (45).

TABLE 7
Mulliken Overlap Populations (MOP) for $Nb_{28}Ni_{33.5}Sb_{12.5}$

Contact	Distances (Å)	MOP
Nb–Nb	2.488(2)	0.550
	2.736(1), 2.753(2)	0.417
	2.923(1)–3.324(1)	0.245
	2.488(2)–3.324(1)	0.267
Nb–Ni	2.616(1)–2.998(1)	0.097
Nb–Sb	2.8786(9)–2.9881(9)	0.271
Ni–Ni	2.360(2)–2.674(2)	0.050
Ni–Sb	2.4833(9)–2.5915(8)	0.222

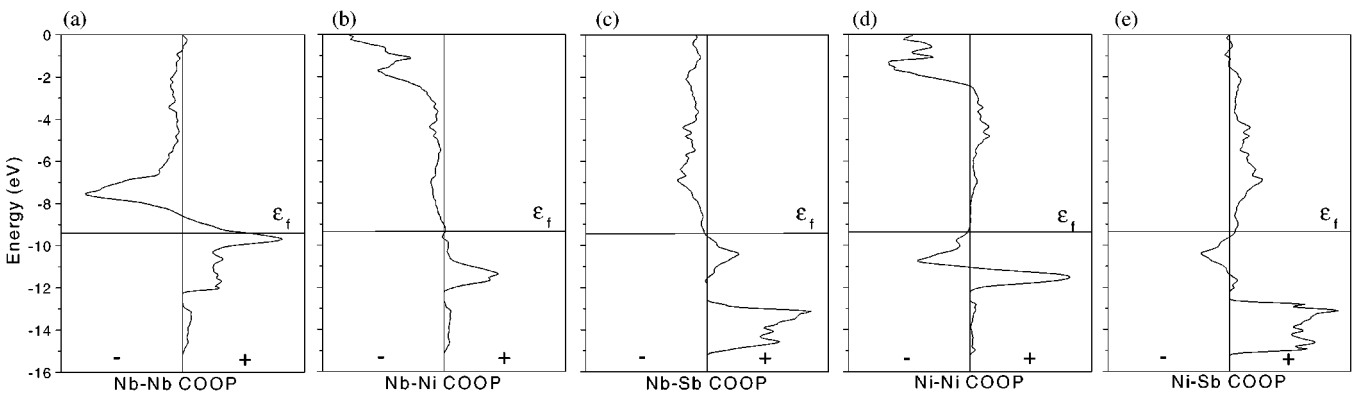

FIG. 6. Crystal orbital overlap population (COOP) curves for (a) Nb–Nb, (b) Nb–Ni, (c) Nb–Sb, (d) Ni–Ni, and (e) Ni–Sb contacts, within the range of distances listed in Table 7, in $Nb_{28}Ni_{33.5}Sb_{12.5}$ (idealized as "$Nb_{28}Ni_{32}Sb_{14}$").

ACKNOWLEDGMENTS

This work was supported by the Natural Sciences and Engineering Research Council of Canada and the University of Alberta. We thank Dr. Michael J. Ferguson and Dr. Robert McDonald (Faculty Service Officer, X-ray Crystallography Laboratory) for the data collection and Christina Barker for assistance with the EDX analysis.

REFERENCES

1. "Handbook of Crystal Structures and Magnetic Properties of Rare Earth Intermetallics" (A. Szytuła and J. Leciejewicz, Eds.). CRC Press, Boca Raton, FL, 1994.
2. B. C. Sales, D. Mandrus, and R. K. Williams, *Science* **272,** 1325 (1996).
3. H. Kleinke, *Z. Anorg. Allg. Chem.* **624,** 1272 (1998).
4. A. E. Dwight, *Mater. Res. Bull.* **22,** 201 (1987).
5. W. Rieger and E. Parthé, *Acta Crystallogr., Sect. B: Struct. Crystallogr. Cryst. Chem.* **24,** 456 (1968).
6. E. Garcia and J. D. Corbett, *Inorg. Chem.* **29,** 3274 (1990).
7. Y.-U. Kwon, S. C. Sevov, and J. D. Corbett, *Chem. Mater.* **2,** 550 (1990).
8. H. Kleinke, C. Ruckert, and C. Felser, *Eur. J. Inorg. Chem.* 315 (2000).
9. H. Kleinke, *J. Alloys Compd.* **270,** 136 (1998).
10. M. Wang, R. McDonald, and A. Mar, *Inorg. Chem.* **38,** 3435 (1999).
11. E. Garcia and J. D. Corbett, *J. Solid State Chem.* **73,** 440 (1988).
12. E. Garcia and J. D. Corbett, *J. Solid State Chem.* **73,** 452 (1988).
13. L. F. Myzenkova, V. V. Baron, and Ye. M. Savitskiy, *Russ. Metall.* (*Engl. Transl.*) 89 (1966).
14. A. Kjekshus, *Acta Chem. Scand.* **26,** 1633 (1972).
15. S. Furuseth and A. Kjekshus, *Acta Crystallogr.* **18,** 320 (1965).
16. A. Rehr and S. M. Kauzlarich, *Acta Crystallogr., Sect. C: Cryst. Struct. Commun.* **50,** 1177 (1994).
17. E. Garcia and J. D. Corbett, *Inorg. Chem.* **27,** 2353 (1988).
18. S. Furuseth and A. Kjekshus, *Acta Chem. Scand.* **18,** 1180 (1964).
19. K. Schubert, A. Raman, and W. Rossteutscher, *Naturwissenschaften* **51,** 506 (1964).
20. B. G. Hyde and S. Andersson, "Inorganic Crystal Structures." Wiley, New York, 1989.
21. F. C. Frank and J. S. Kasper, *Acta Crystallogr.* **11,** 184 (1958).
22. F. C. Frank and J. S. Kasper, *Acta Crystallogr.* **12,** 483 (1959).
23. J. H. Wernick, *in* "Intermetallic Compounds" (J. H. Westbrook, Ed.), p. 197. Wiley, New York, 1967.
24. C. B. Shoemaker and D. P. Shoemaker, *in* "Developments in the Structural Chemistry of Alloy Phases" (B. C. Giessen, Ed.), p. 107. Plenum Press, New York, 1969.
25. Ya. P. Yarmolyuk, P. I. Kripyakevich, and E. I. Gladyshevskii, *Sov. Phys. Crystallogr.* (*Engl. Transl.*) **15,** 226 (1970).
26. P. C. Manor, C. B. Shoemaker, and D. P. Shoemaker, *Acta Crystallogr., Sect. B.: Struct. Crystallogr. Cryst. Chem.* **28,** 1211 (1972).
27. G. M. Sheldrick, "SHELXTL," Version 5.1, Bruker Analytical X-ray Systems, Inc. Madison, WI, 1997.
28. "International Tables for X-ray Crystallography" (A. J. C. Wilson, Ed.), Vol. C. Kluwer, Dordrecht, 1992.
29. J. S. Kasper, *in* "Theory of Alloy Phases," p. 264. American Society for Metals, Cleveland, OH, 1956.
30. L. M. Gelato and E. Parthé, *J. Appl. Crystallogr.* **20,** 139 (1987).
31. M.-H. Whangbo and R. Hoffmann, *J. Am. Chem. Soc.* **100,** 6093 (1978).
32. R. Hoffmann, "Solids and Surfaces: A Chemist's View of Bonding in Extended Structures." VCH Publishers, New York, 1988.
33. H. Kleinke and H. F. Franzen, *J. Am. Chem. Soc.* **119,** 12824 (1997).
34. D. P. Shoemaker and C. B. Shoemaker, *Acta. Crystallogr., Sect. B: Struct. Sci.* **42,** 3 (1986).
35. Yu. B. Kuz'ma, *Russ. J. Inorg. Chem.* (*Engl. Transl.*) **7,** 691 (1962).
36. J. Donohue, "The Structures of the Elements." Wiley, New York, 1974.
37. A. Kjekshus and K. P. Walseth, *Acta Chem. Scand.* **23,** 2621 (1969).
38. L. Pauling, "The Nature of the Chemical Bond," 3rd ed. Cornell Univ. Press, Ithaca, NY, 1960.
39. J. H. Carpenter and A. W. Searcy, *J. Am. Chem. Soc.* **78,** 2079 (1956).
40. F. A. Cotton, J. H. Matonic, and C. A. Murillo, *J. Am. Chem. Soc.* **120,** 6047 (1998).
41. A. Kaufman, N. J. Hoffman, and H. Lipson, *Scr. Metall.* **3,** 715 (1969).
42. S. Andersson, *J. Solid State Chem.* **23,** 191 (1978).
43. T. Hughbanks and R. Hoffmann, *J. Am. Chem. Soc.* **105,** 3528 (1983).
44. P. Pyykkö, *Chem. Rev.* **97,** 597 (1997).
45. S. Lee, *J. Am. Chem. Soc.* **113,** 101 (1991).